Journal of Materials Chemistry C

Adaptive coloration enabled by the reversible osmotic annealing of chromatophore-like microcapsules

Journal:	*Journal of Materials Chemistry C*
Manuscript ID	TC-ART-10-2023-003824.R1
Article Type:	Paper
Date Submitted by the Author:	22-Dec-2023
Complete List of Authors:	Kim, Jae-Hyun; Sungkyunkwan University, School of Chemical Engineering Lee, Ji-Young; Northeastern University - Boston Campus Kim, Jaekyoung; University of Pennsylvania Gong, Zhe; University of Pennsylvania, Chemical and Biomolecular Engineering Wilson, Daniel; Northeastern University - Boston Campus Deravi, Leila; Northeastern University, Chemistry and Chemical Biology Lee, Daeyeon; University of Pennsylvania,

SCHOLARONE™
Manuscripts

ARTICLE

Adaptive coloration enabled by the reversible osmotic annealing of chromatophore-like microcapsules†

Received 00th January 20xx,
Accepted 00th January 20xx

DOI: 10.1039/x0xx00000x

Jae-Hyun Kim,‡[a] Ji-Young Lee,‡[b] Jaekyoung Kim,‡[a] Zhe Gong,[a] Daniel J. Wilson,[c] Leila F. Deravi*[b] and Daeyeon Lee*[a]

Nature's diverse creatures have evolved sophisticated mechanisms via molecules, nanostructures, yielding dynamic and brilliant biological color transformations. Inspired by these systems, we generate a dynamic soft system that facilitates reversible selection between predominately pigment-based or structure-based mechanisms of coloration via actuation through changes in osmotic pressure. To achieve this, we use microfluidics to prepare double emulsion capsules which encapsulate polystyrene nanoparticles functionalized with xanthommatin, a biochrome. This system enables controlled modulation between color mechanisms through pigment loading density and osmotic stress manipulation, offering finely-tuned color changes in the double emulsion capsules. We further investigate the relationship between these two coloration mechanisms by comparing the reflectance spectra of chromatophore-like capsules and demonstrate a material system that can house the capsules and elicit bulk color changes. Our results highlight a unique and potentially scalable approach for fabricating color-changing materials that provide access to a broad range of tunable visible colors.

Introduction

Across nature, colors spanning the visible spectrum are produced by sophisticated manipulations of light by absorptive molecules and structures that lead to optical interference. This broad diversity in visible appearances has evolved in both the plant and animal kingdoms, stemming from a variety of biological needs and correlating with a multitude of mechanisms of color change that operate across a wide range of spectrum and timescales.[1, 2] Cephalopods provide a vivid example of this phenomenon, having the ability to undergo dramatic changes in color, pattern, and shape in response to environmental stimuli using pigments, structure, and combinations of both.[3-5] To execute such dynamic display, these animals rely on a synergistic use of specialized organs containing pigmented granules called chromatophores,[6, 7] underlying Bragg stack reflectors called iridophores,[8] and, in some species, diffuse light scattering components known as leucophores.[9] Within cephalopod skin, these components operate in concert to enable large-scale, dramatic alterations of color and pattern. A specific example can be observed in the squid Doryteuthis pealeii, where angle-dependent structural coloration has been observed to emerge in precise synchronization with actuation of pigmentary chromatophores, inspiring several applications in materials science.[2, 7, 10] However, an outstanding challenge in approximating the display performance demonstrated by cephalopods using engineered materials lies in creating technologies that are capable of complementary actuation of pigmentary and structural coloration mechanisms.

While many color-changing technologies have been developed using pigments as active components, including approaches based on translocation of colored solutions[11] or electrochromism,[12, 13] these actuation strategies (e.g., pressure, electricity) are not entirely compatible with the stimuli used to specifically target patterned features of tunable structural materials, which can include humidity,[14] organic vapors,[15] pH,[16] temperature,[17] and mechanical force.[18] To develop engineered systems capable of actuation across diverse coloration mechanisms, similar to the performance exemplified by cephalopods, a strategic selection of materials must be made that can respond to common or compatible stimuli. In recent years, strides have been made in this area, particularly with photonic materials prepared from colloids, demonstrated to produce colors that span the entire visible spectrum.[19-24] This class of materials also includes synthetic photonic pigments fabricated in spherical microcapsules, which can be manufactured rapidly via microfluidics and geometrically reconfigured using osmotic stress.[19, 25-27]

In an effort to bridge the gap between independent actuation of engineered pigmentary or structural coloration materials and the integrated, comprehensive function of the biological color organs distributed throughout cephalopod skin, we design and fabricate color-switchable colloidal assemblies confined within water-oil-water (W/O/W) double emulsion capsules controlled by osmosis. By coupling the primary pigment found in the granules of cephalopod chromatophores, xanthommatin (Xa),[6, 7, 28] to polystyrene particles contained within the inner water phase

[a] Department of Chemical and Biomolecular Engineering, University of Pennsylvania, Philadelphia, PA 19104, United States
[b] Department of Chemistry and Chemical Biology, Northeastern University, Boston, MA 02115, United States
[c] Kostas Research Institute, Northeastern University, Burlington, MA 01803, United States

† Electronic Supplementary Information (ESI) available: See DOI: 10.1039/x0xx00000x.

‡ These authors contributed equally to this work.

of these microcapsules, we observe characteristic pigmentary color when the particles are freely dispersed in the unstrained capsule. Upon introduction of osmotic stress across the selectively permeable oil shell of the double emulsion capsules, we observe structural color that is dependent on the osmotic annealing conditions and presence of pigment within the system. While numerous studies have focused on inducing structural color by shrinking microcapsules, they have largely overlooked the potential for reversible control of photonic properties through both shrinkage and expansion. This current study marks a significant advancement: we develop microcapsules capable of exhibiting reversible coloration, a novel mechanism achieved through precise modulation of osmotic annealing conditions. In all cases, osmotically induced actuation of the capsules is reversible, and in the case of the pigment-containing system, we are able to combine pigmentary and structural coloration using a common stimulus. Furthermore, we fabricate an artificial skin by embedding these adaptive chromatophore-like microcapsules in a hydrogel matrix which can also be reversibly actuated by osmosis to reveal changes in size and color. Taken together, our findings represent an important step toward emulating the comprehensive function of coloration organs in cephalopod skin using engineered systems.

Results and discussion

Reconfigurable photonic microcapsules

Inspired by soft actuating systems like the cephalopod chromatophores, we design, build, and test double-emulsions containing polystyrene (PS) nanoparticles in the core of a water-in-oil-in-water (W/O/W) microcapsule. We and others have shown that applying osmotic pressure difference between the inner and outer phases of double emulsions can lead to diffusion of water out of the inner phase to induce shrinkage of the inner phase.[19, 25-27] When PS nanoparticles are present in the inner phase, they undergo assembly to exhibit structural color. However, few studies have shown that this process could be reversed to dissemble the features of structural coloration in these soft systems, and thus we test this possibility.

Monodisperse W/O/W double emulsion capsules are produced using a glass capillary microfluidic device.[29] The inner aqueous phase is composed of PS nanoparticles (2.5 w/w%) suspended in a PVA solution (0.5 wt.%) that is encapsulated within a fluorocarbon (FC) oil (HFE-7500) middle phase upon injection into an outer aqueous phase (Fig. 1a, b). The middle and outer phases have 1 wt.% surfactant (Krytox 157FSH) and 5wt.% PVA, respectively, to stabilize the double emulsion capsules. By collecting these double emulsion capsules in an aqueous NaCl solution, we create an osmotic imbalance across the oil shell to force the shrinkage of the inner aqueous phase and packing of PS nanoparticles (Fig. 1c, d). Over the course of one hour in a 2.5 M NaCl solution, PS nanoparticles in the inner phase organize into colloidal assembly with an angle-independent diffuse blue-green color (Fig. 1d and Fig. S1a, ESI†). We conduct various NaCl concentrations (0 M to 2.5 M) and observe that the time it takes to complete osmotic annealing is dictated by the concentration of PS nanoparticles in the aqueous core and the osmotic pressure gradient across the oil shell, which is controlled by the salt concentration of the outer bulk solution (Fig. S1a, ESI†).

Because the physical reorganization of PS nanoparticles within the inner phase of microcapsules is driven by an osmotic pressure imbalance across the oil shell, the formation of structural color should be fully reversible by exposing the annealed double emulsion capsules to hypotonic conditions as illustrated in Fig. 1c. Addition of osmolyte to the inner phase of double emulsions facilitates the swelling of the inner phase and, in turn, the osmotic melting of the colloidal assembly that formed after osmotic annealing. However, the addition of salt such as NaCl in the inner phase is not desirable, as shrinkage of the inner phase via osmotic annealing would significantly increase its ionic strength and jeopardize the colloidal stability of PS nanoparticles which are electrostatically stabilized. To avoid this problem, we add 50 mM sucrose to the inner phase during production. Sucrose is a non-ionic compound and has a low permeability through the FC oil shell and does not significantly alter the colloidal stability of PS nanoparticles during annealing. However, the presence of sucrose and PVA reduces the osmotic pressure differences between phases, which slows the overall annealing process. Furthermore, optical reflection mode microscope images of annealed photonic cores with and without sucrose exhibit distinct color appearances (Fig. S2, ESI†). The inner phase with sucrose displays blue-green colors, whereas those without sucrose display a blue color. These results are consistent with the angle independent structural color of our PS nanoparticles, which have a measured diameter of 170 nm through SEM analysis and an associated blue color.[19, 30] This colorimetric shift is an effect of the added sucrose, which leads to a reduction in the packing fraction compared to samples without sucrose. This effect results in a blue-green color appearance and a larger inner phase diameter after osmotic annealing.

Expansion of the inner phase is achieved by replacing the NaCl solution that was used to achieve osmotic compression with an aqueous solution of PVA (2.5 wt.%) with no added salt. We observe osmotic expansion of the double emulsion capsules and the disappearance of structural color due to dispersion of PS nanoparticles in the inner aqueous phase of the double emulsion capsules as shown in Fig. 1d. By cyclically exposing the PS nanoparticle-containing double emulsion capsules to hypertonic and hypotonic conditions, we observe reversible elimination and restoration of structural color.

Reconfigurable chromatophore-like microcapsules

Inspired by the combinations of pigmentary and structural color that enable cephalopods to perform drastic transformation of their visible appearance, we couple the xanthommatin (Xa), the primary pigment in cephalopod chromatophores, to polystyrene particles with low pigment loading density (Xa1) and high pigment loading density (Xa2) and encapsulate these pigmented nanoparticles in double emulsion capsules to investigate how its presence impacts colors emanating from these dynamically

This journal is © The Royal Society of Chemistry 20xx

Please do not adjust margins

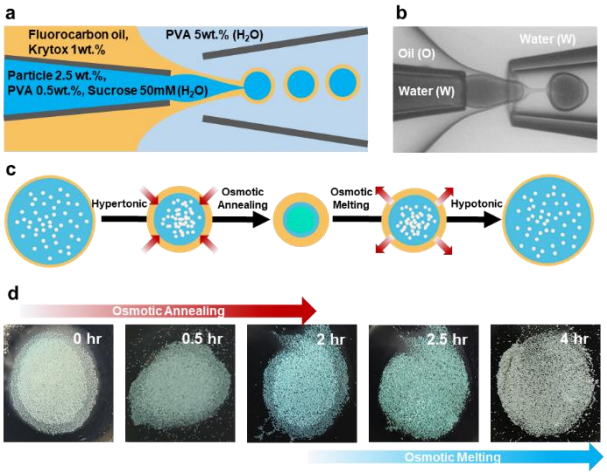

Fig. 1. Fabrication of osmosis induced reversibly color changeable photonic capsule. a) Schematic illustration of fabrication of chromatophore-like capsule by microfluidic system, b) Optical image of chromatophore-like capsule fabrication in a glass capillary based-microfluidic device. c) Schematic illustration of reverse osmosis annealed photonic capsule, d) Photograph of reversible annealing of chromatophore-like capsules under hypertonic (NaCl 2.5M) and hypotonic (NaCl 0M) conditions. Microcapsules prepared using unfunctionalized white nanoparticles (PS) provide blue-green amorphous structural color upon osmotic compression.

tunable artificial chromatophores. Fig. 2 show the optical microscope transmission and reflection mode images of non-annealed and annealed microcapsules with PS, Xa1, and Xa2 particles. Additionally, the optical images of annealed microcapsules under various salt concentrations are shown in Fig S1 (ESI†). Xa has a high refractive index (1.73–2.09),[31] and a broad absorbance profile with an absorbance maximum around 440 nm in the oxidized form (Fig. S3, ESI†). These features contribute in part to the changes in reflectivity and transmittance from the osmotically manipulated double emulsion capsules. Specifically, chemically coupling Xa to the carboxylated PS nanoparticles using the 1-ethyl-3-(3-dimethylaminopropyl) carbodiimide (EDC) reaction shifts the visible color of the originally white particle suspension within the fabricated double emulsion capsules to tan/brown (Fig. S4 and Fig. S5, ESI†) without appreciably changing nanoparticle diameter or size distribution. Double emulsion capsules containing the Xa-functionalized nanoparticles in the inner aqueous phase show a uniform yellow color characteristic of the oxidized form of the pigment. After osmotic annealing, double emulsions containing unfunctionalized PS nanoparticles display a diffuse blue-green color (Fig. 2a). In contrast, annealed double emulsions prepared with Xa1 nanoparticles display a faint yellow-green hue (Fig. 2b), likely resulting from a combination of green structural color and the compaction of pigment-bearing nanoparticles. With Xa2 nanoparticles, brown color characteristic of concentrated oxidized Xa dominates the visible appearance of these chromatophore-like microcapsules resulting in yellow-green color after osmotic annealing (Fig. 2c).

We characterize these qualitative color changes by measuring the reflectance spectra of individual double emulsion capsules. The reflectance spectra of double emulsion capsules containing these Xa-functionalized nanoparticles before and after osmotic annealing reveal that nanoparticles dispersed throughout the inner aqueous phase randomly scatter light prior to annealing, as demonstrated by a broad reflectance profile. Upon osmotic annealing, the distance between particles gradually decreases and a structural color peak emerges at 494 nm across all conditions, albeit with a varying peak distribution depending on pigment abundance (Fig. S6, ESI†). Specifically, the deconvoluted reflectance spectra reveal that the structural peak for PS at 494 nm is more narrow; whereas, the Xa1 and Xa2 conditions produce a broadened peak, indicating more diffuse color. Xa1 and Xa2 exhibit pigmentary peaks at 664 nm. Furthermore, the presence of the Xa also influences the packing arrangement of functionalized particles. This is not surprising, given that the zeta potential of the pigment functionalized nanoparticles, Xa1 and Xa2, are around -9.6 mV and -7.4 mV, respectively, whereas the unfunctionalized particles is around -52 mV (Table S1, ESI†). We confirm that particles form disordered assemblies after osmotic annealing in all PS, Xa1, and Xa2 through SEM imaging (Fig. S7, ESI†). Additionally, analysis of the deconvoluted reflectance spectra of the three types of microcapsules indicates that as the Xa loading density increases, the structural peak intensity decreases and broadens. It is well known that structural color depends on the volume fraction of particles, the diameter of particles, and the refractive indices of the particles and the medium.[19, 27, 32] In our experiments, the refractive index of the particle remains constant during osmotic annealing, whereas the volume fraction of particles (ϕ) and refractive index of medium in the inner phase of double emulsion change. The volume fraction of particles in the inner phase of double emulsion (ϕ (t)), which varies as a function of time, can be estimated using:[27]

$$\phi(t) = \phi_0 \left(\frac{R_0 - l_0}{R(t) - l(t)}\right)^3 \quad (1)$$

$$l(t) = R(t) - \left\{R(t)^3 - {R_0}^3 + (R_0 - l_0)^3\right\}^{1/3} \quad (2)$$

where R is the radius of the double emulsion capsules, and l is the middle phase (oil phase) shell thickness. Subscript 0 indicates the initial state. After 120 min, double emulsion capsules containing Xa2 particles have the normalized radius of 0.55 ± 0.02 and ϕ = 0.53 ± 0.11, maintaining a similar volume fraction even after 24 hours (Fig. 3b and Fig. S8, ESI†). The densest packing of nanoparticles attainable in these double emulsion capsules is 0.74, assuming a close-packed arrangement with face-centered cubic (FCC) structure. However, the presence of sucrose in the inner phase reduces the osmotic pressure imbalance between the inner and the outer phases, resulting in a reduced volume fraction. The nanoparticles are initially dispersed in the inner phase consisting of 0.5 wt% PVA and 50 mM sucrose. After annealing, the concentrations of sucrose and PVA in the inner phase become approximately 1 M and 11 wt.%, respectively, raising the refractive index of this medium to 1.4. The calculated wavelength of the Bragg reflection (λ) using equations for photonic crystal[19, 27, 32] and photonic glass structure[33, 34] is in range of 444 - 495 nm and 412 - 495 nm, respectively (Equation Section, ESI†). This finding aligns with our experimental data which reveals a structural color peak at

Please do not adjust margins

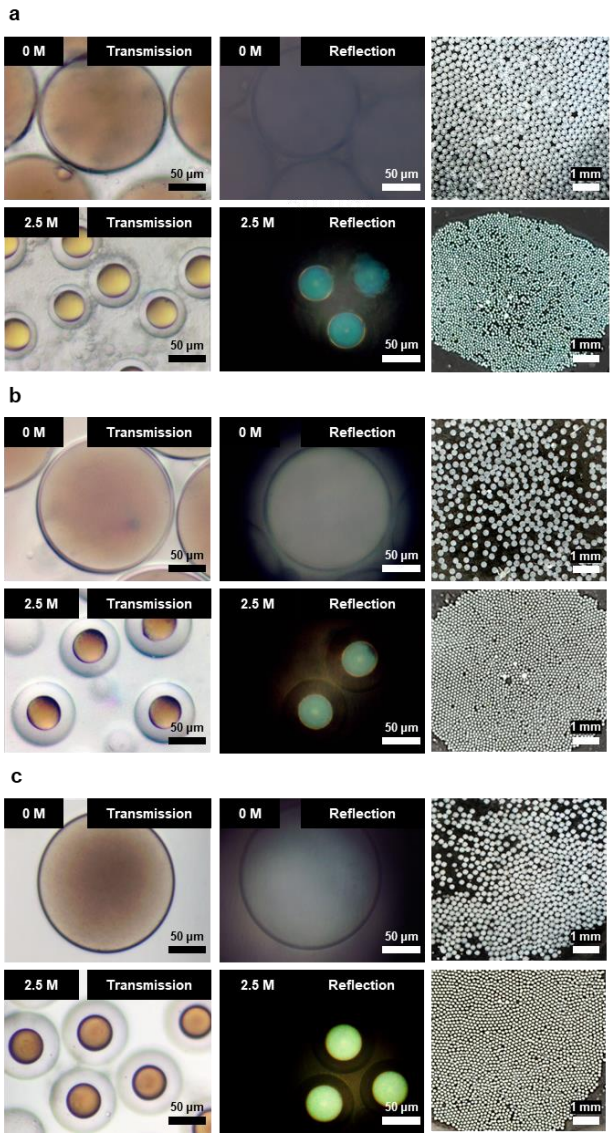

Fig. 2. Understanding the contributions of pigments on structural colors. a-c) Optical microscope image (transmission mode and reflection mode) and optical image of double emulsion capsules containing a) PS particles, b) Xa1 particles, and c) Xa1 particles annealed by 2.5 M salt concentration. The upper and bottom layers represent capsules before and after osmotic annealing.

494 nm through deconvolution across all conditions. Also, we note a pigmentary peak at 664 nm, both before and after annealing, in microcapsules in both Xa1 and Xa2 particles (Fig. 3a and Fig. S6, ESI†). Upon increasing the pigment loading density, a pigmentary color becomes more dominant and distinct.

Similar to double emulsions containing unfunctionalized PS nanoparticles, double emulsion capsules prepared using Xa-functionalized particles can undergo repeated cycles of reversible osmotic compression and expansion. This allows for switching between pigmentary color (brown) and structural color (yellow-green) mechanisms, as shown in Fig. 3c. Overall, these results demonstrate that by encapsulating Xa-functionalized nanoparticles in double emulsion capsules which are subsequently osmotically annealed, we can modulate the resulting colors without changing the size of encapsulated nanoparticles. Importantly, the accessible color palette for these

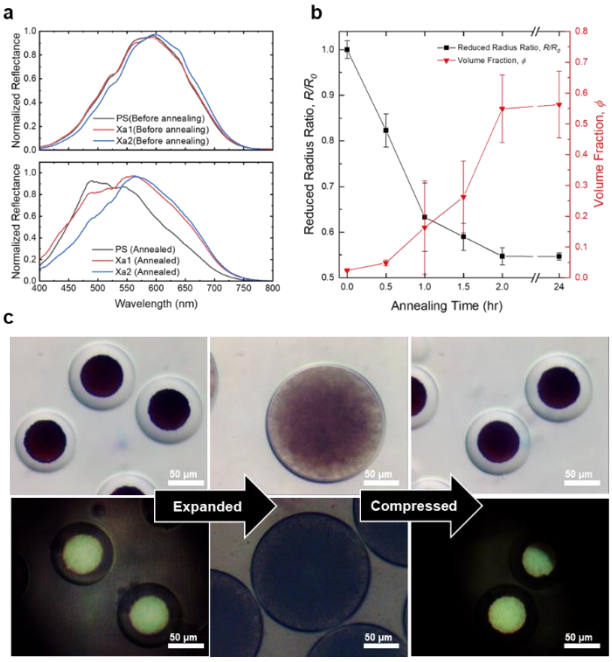

Fig. 3. Switching between pigmentary and structural coloration. (a) Reflectance spectra are measured before and after annealing of PS and Xa-coupled nanoparticles (Xa1 and Xa2) double emulsion capsules. (b) Normalized radius (R/R0) of Xa2 particle-containing double emulsion capsules in NaCl 2.5 M and Xa2 volume fraction inside the inner phase as a function of annealing time. The volume fraction and normalized radius of Xa2 particle-containing double emulsion capsules as a function of annealing time is obtained by analyzing five double emulsion capsules and the standard deviation of these five measurements is used for error bars. (c) Osmosis-controlled switching between expanded in NaCl 0 M and compressed states in NaCl 2.5 M.

Xa-functionalized nanoparticles provides a brown hue to expanded double emulsions that shift based on pigment loading density when the double emulsion contracts.

Fabrication of hydrogel with chromatophore-like microcapsules

Inspired by the skin of cephalopods, we prepare a free-standing slab containing the double emulsions by physically embedding them into the cross-linked network of the poly (ethylene glycol) diacrylate (PEGDA) as illustrated in Fig. S9 (ESI†), and Experimental section. We use a photoinitiator, lithium phenyl-2,4,6-trimethylbenzoylphosphinate (TPO-Li) to polymerize the PEGDA,[35] which encases the double emulsion capsules (Fig. 4a). Upon UV-crosslinking the hydrogel, we observe excellent stability of the capsules (Fig. S10, ESI†), which retain their sensitivity to osmotic pressure imbalance to produce bulk color changes (Fig. 4b-d). The capsules embedded in the hydrogel matrix show enhanced physical stability compared to freely suspended double emulsion microcapsules in salt solutions. A surfactant such as PVA is necessary to maintain the stability of double emulsion microcapsules in salt solutions; however, the double emulsions in the hydrogel remain stable in salt solution without the surfactant as the hydrogel matrix keep the double emulsion capsules physically separated at all times. The chromatophore-like microcapsules embedded in the hydrogel artificial skin undergo osmotic compression within an aqueous solution with a 2.5M NaCl concentration. An optical microscope

This journal is © The Royal Society of Chemistry 20xx

Please do not adjust margins

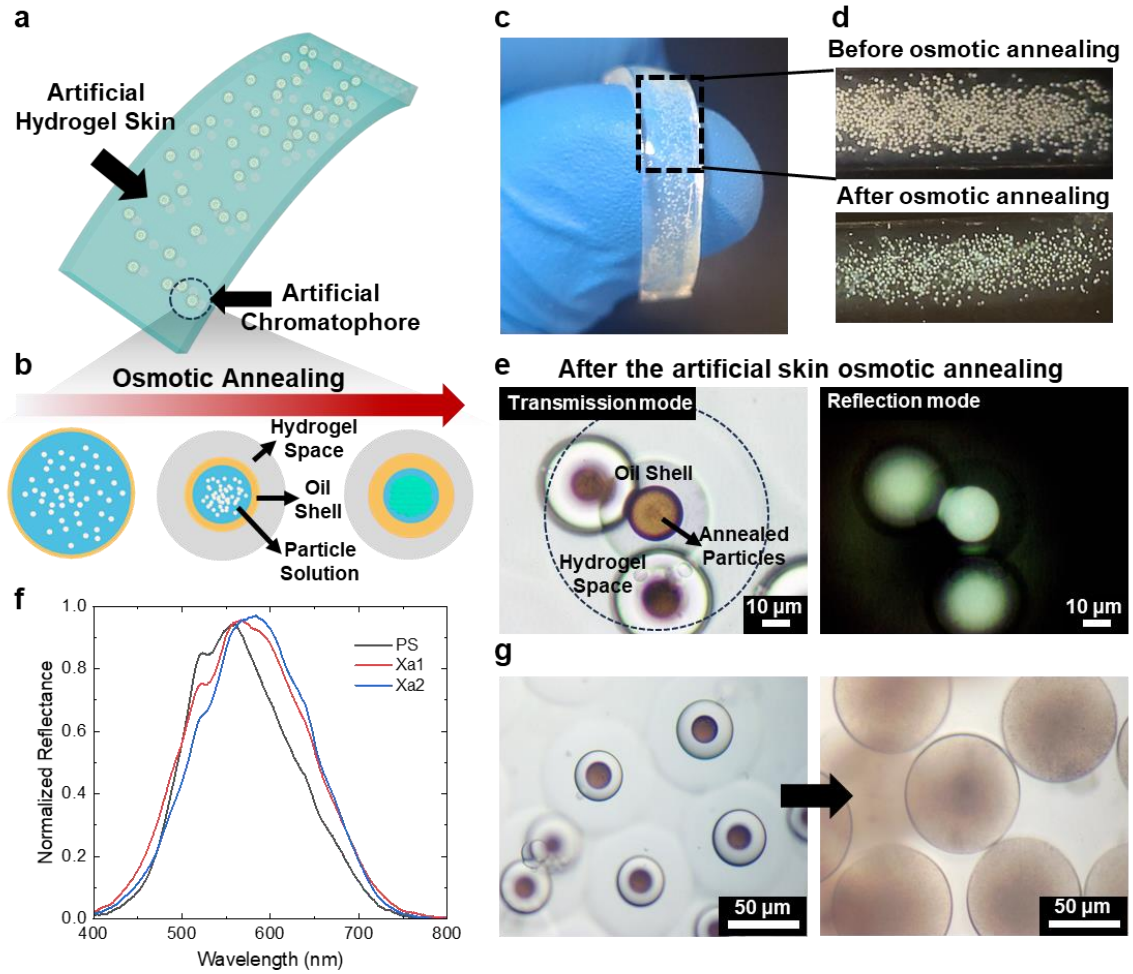

Fig. 4. Fabrication of artificial cephalopod skin by hydrogel. (a) A schematic representation of cephalopod inspired hydrogel. Hydrogel containing Xa2 particle-containing double emulsion capsules fabricated first and then mixed with PEGDA, UV-crosslinker aqueous solution. (b) A schematic of osmotic annealing double emulsion capsules in hydrogel. (c) Macroscopic image of artificial chromatophore, and (d) images of before and after osmosis annealing. (e) Optical microscope images of osmosis annealing of double emulsion capsule in hydrogel. (f) Reflectance spectra of annealed bare PS, Xa1 and Xa2 particle-containing double emulsion capsules in the hydrogel matrix. (g) Optical microscope images showing the expansion of chromatophore-like microcapsules in the hydrogel matrix.

image of the Xa2 hydrogel in Fig. 4e reveals that the double emulsion capsules undergo shrinkage upon osmotic annealing while retaining their original morphology to produce a chromatic transition from a tan-yellow color to a faint yellow-green hue. The spectra of the annealed composite prepared with double emulsion capsules containing the three types of particles are exhibited in Fig. 4f. To evaluate the impact of the hydrogel matrix on microcapsule annealing, we measure the swelling and deswelling ratio for PEGDA hydrogel and microcapsules embedded in the hydrogel (Fig. S11a, ESI†). When we compare their sizes after soaking in a 2.5 M NaCl with 2.5 wt.% PVA, we observe that the hydrogel deswell by 10%, while the microcapsules in the hydrogel shrink by 80%. Upon rehydration in the absence of salt, the hydrogel swell by 7%, and the capsules in the hydrogel expand by 4%, compared to their initial states. These changes in microcapsule annealing behavior correspond to different optical properties. Specifically, the structural color peak of PS, Xa1, and Xa2 in the hydrogel is observed around 530 nm by deconvolution analysis which is red-shifted from microcapsules in solution (494 nm, Fig. S6, ESI†). We believe this difference is due to the presence of the hydrogel matrix which may reduce the osmotic annealing force (Fig. S11b, ESI†). Also, the capsules embedded in the hydrogel matrix experienced a rapid reduction in radius within 1 hour, and after 2 hours, they reach their fully annealed state and remain stable at least for 1 day (Fig. S11b, ESI†). These microcapsules can be expanded back to the original state by exposing the hydrogel composite to pure water as shown in Fig. 4g, emulating the reversible color-changing capabilities of cephalopod skin.

Conclusions

In conclusion, the collaborative display of pigmentary and structural coloration in cephalopods enables rapid, dramatic changes in color, pattern, and visible appearance over spatial scales orders of magnitude larger than chromatophores and underlying structural reflectors. A major obstacle in creating engineered systems that approach the impressive capabilities of these natural systems hinges on the fabrication of selectively actuated pigmentary and structural display features that can be packaged or arrayed together to offer synergistic optical

This journal is © The Royal Society of Chemistry 20xx

Please do not adjust margins

functions. In this work, we present microcapsules that can be osmotically reconfigured to leverage pigmentary or structural color on-demand. These microcapsules exhibit reversible color-switching characteristics, achieved through the shrinking and expansion of microcapsules via osmotic pressure modulation. In expanded double emulsion microcapsules, pigment-functionalized particles are uniformly dispersed throughout the inner aqueous phase to provide uniform absorbance-based color. As nanoparticles are physically rearranged to provide structural color, the concentration of absorptive pigment molecules present on the surface of the nanoparticles modulates the hue and saturation of the resulting colloidal architecture. While these microcapsules are currently actuated via global changes in the surrounding environment, fabrication of independently addressable "pixels" capable of providing multiple forms of pigmentary and structural color presents new and unique opportunities for investigations of cooperative interactions between these fundamentally different coloration mechanisms, as well as development of future adaptive display technologies.

Experimental details

Synthesis of Xanthommatin functionalized nanoparticles

We synthesized xanthommatin (Xa) via cyclization of 3-hydroxykynurenine using a modification of previous procedures.[36-38] 3-hydroxykynurenine (4 mg, 0.018 mmol, 1.00 equiv) was suspended in 1 mL DI H_2O and dissolved by 30 µL of 1 M NaOH Potassium ferricyanide (16.5 mg, 0.05 mmol, 2.78 equiv) was dissolved in 0.5 mL DI H_2O and added dropwise to the 3-hydroxykynurenine solution. The reaction was covered to exclude light and stirred at room temperature for 1.5 hours. The product was precipitated using 90 µL of 1 M hydrochloric acid (HCl), washed 3 times with chilled DI H_2O, and stored at 4 °C. To create pigment functionalized particles, we used carbodiimide chemistry to Xa to access carboxyl groups on the surface of polystyrene nanoparticles (PS). Particles were purchased from a commercial vendor (Polysciences Inc., cat. no. 08216, 4 % coefficient of variance). Concentrated nanoparticle stocks (2.5% w/v) were used to achieve high and low coverage densities of Xa on the surfaces of the nanoparticles. For coupling the Xa to polystyrene particles, 100 µL of 1 % sodium dodecyl sulfate (SDS) solution was added to a vial containing 2 mL of carboxyl-functionalized polystyrene nanoparticles. 1 mL of a 10 mg/mL solution of 1-ethyl-3-(3-dimethylaminopropyl) carbodiimide (EDC) in 0.1 M MES (4-morpholineethanesulfonic acid) buffer pH 5.5 was added to the PS and stirred at room temperature for 30 min. Next, for low density (Xa1) and high-density (Xa2) pigment loading, 5 mL of 0.8 mg/mL and 5 mL of 2 mg/mL Xa reaction product in MES buffer was added to the reaction, respectively. Then, stirred for 2 hr at room temperature and the functionalized particles were washed with DI H_2O 3 times by centrifugation, then stored in DI H_2O at 4 °C.

Fabrication of chromatophore-like microcapsules

Chromatophore-like microcapsules containing bare PS nanoparticles and Xa-functionalized PS particles (Xa1 and Xa2) were fabricated using a glass capillary-based microfluidic device. We prepared water-in-oil-in-water (W/O/W) double emulsions according to a previously described method[19] using injection and collection capillaries with 120 µm and 200 µm diameters, respectively. To generate the W/O/W double emulsions, an aqueous suspension of PS (2.5 wt.%) was injected through an oil phase into water. The middle oil phase consisted of hydrofluoroether oil (HFE 7500, 3M) containing 1 wt.% surfactant (Krytox 157FSH, DuPont). The outer aqueous bulk fluid contained 5 wt. % poly(vinyl alcohol) (PVA, 87-89% hydrolyzed, average Mw = 13,000–23,000, Sigma Aldrich) aqueous solution. The flow rates for the inner (i.e., aqueous suspension of PS nanoparticles), middle (i.e., fluorocarbon oils), and outer (i.e., aqueous PVA solutions) fluids were set at 6 mL/h, 2.5 mL/h, and 30 mL/h, respectively. Formation of double emulsion capsules was monitored and recorded using an inverted microscope (Nikon Diaphot 300) with a high-speed camera (Phantom V7.1). Double emulsion capsules were collected in aqueous NaCl solutions with controlled osmolarity to induce osmotic annealing.

Reversible compression and expansion of elastic chromatophore-like microcapsules

To induce osmotic compression, double emulsion capsules were collected in a 2.5 wt.% PVA dissolved concentrated aqueous NaCl solution and left undisturbed. Depending on the osmotic pressure across the semi-permeable oil shell of the capsules, we observed annealing times ranging from 1 hour to several hours (i.e., 4-6 hrs) required for nanoparticles to pack and maintain their structural coloration. For osmotic expansion, we added sucrose (Sigma-Aldrich) to the inner phase, enabling a reverse osmotic process. We carefully removed the initial NaCl solution and replaced it with a 2.5 wt.% PVA solution to create a hypotonic environment. To monitor cycling between osmotic compression and expansion, capsules were imaged in hypertonic or hypotonic environments using an optical microscope every 30 mins until their size remained constant, signifying a final equilibrium geometry. Once the capsules achieved the equilibrium state, the surrounding bulk solution was replaced to shift the central capsule toward the appropriate nanoparticle configuration.

Fabrication of hydrogel

Poly(ethylene glycol) diacrylate (PEGDA, Mn = 700, Sigma Aldrich, St. Louis, MO, USA), lithium phenyl-2,4,6-trimethylbenzoylphosphinate (TPO-Li, Sigma Aldrich, St. Louis, MO, USA), and deionized water were thoroughly agitated in a 50 ml conical tube and covered to protect the PEGDA pre-polymer solution from UV light exposure. PEGDA (20 wt.%) and 15 mM of TPO-Li were mixed first, followed by the addition of 10% (v/v) of the double emulsion solution to the PEGDA prepolymer without the need for additional surfactant. To prevent double emulsion dewetting upon physical contact, the solution was gently shaken by hand for 10 seconds. A 3D-printed mold (2 cm × 1 cm × 1.2 cm) was employed to control the hydrogel's morphology. 200 µl of the PEGDA and double

This journal is © The Royal Society of Chemistry 20xx

Please do not adjust margins

emulsion mixture was injected into the mold, and photo-crosslinking was initiated using a 370 nm UV light source, with 20 seconds being sufficient for the cross-linking process. The cross-linked double emulsion-embedded hydrogel could then be detached from the mold using tweezers. The detached hydrogel proved to be stable enough to be placed in a NaCl aqueous solution without the addition of surfactants.

Characterization

We measured the size, zeta potential, and absorbance spectrum of PS and Xa-functionalized PS nanoparticles by SEM images (SUPRA 25 SEM, Carl Zeiss), dynamic light scattering (DLS, Malvern Nano-ZS90, Malvern), and UV-vis spectrophotometer (Evolution 220 UV–vis spectrophotometer, Thermo Scientific), respectively. Optical micrographs of the double emulsion capsules and their reflectance spectra were obtained using an upright microscope (Carl Zeiss Axio Plan II) equipped with a CCD camera and a fiber-coupled spectrometer (Laboratory Spectrometer, Edmund Optics).

Author Contributions

J-H.K., J-Y.L., and J.K contributed equally to this work. J-H.K., and D.L. designed and performed the experiments and revised the manuscript; J-Y.L., and L.F.D., analyzed the results and wrote the manuscript; J.K, and Z.G., performed the experiments; D.J.W., L.F.D., and D.L. conceived the experiments; all authors have given approval to the final version of the manuscript.

Conflicts of interest

There are no conflicts to declare.

Acknowledgements

Research was supported by Army Research Office and was accomplished under Cooperative Agreement Number W911NF-22-2-0119. The views and conclusions contained in this document are those of the authors and should not be interpreted as representing the official policies, either expressed or implied, of the Army Research Office or the U.S. Government. The U.S. Government is authorized to reproduce and distribute reprints for Government purposes notwithstanding any copyright notation herein. We also acknowledge Dr. Zhuangsheng Lin and Dr. Rebecca Ford for their initial input on the experiments and materials design, respectively.

References

1 R. C. Duarte, A. A. V. Flores and M. Stevens, *Philosophical Transactions of the Royal Society B: Biological Sciences*, 2017, **372**, 20160342.

2 D. J. Wilson, Z. Lin, D. Q. Bower and L. F. Deravi, *Matter*, 2021, **4**, 2163-2171.

3 J. P. Vigneron, J. M. Pasteels, D. M. Windsor, Z. Vértesy, M. Rassart, T. Seldrum, J. Dumont, O. Deparis, V. Lousse, L. P. Biró, D. Ertz and V. Welch, *Physical Review E*, 2007, **76**, 031907.

4 D. Stuart-Fox and A. Moussalli, *Philosophical Transactions of the Royal Society B: Biological Sciences*, 2009, **364**, 463-470.

5 L. M. Mäthger, M. F. Land, U. E. Siebeck and N. J. Marshall, *Journal of Experimental Biology*, 2003, **206**, 3607-3613.

6 L. F. Deravi, A. P. Magyar, S. P. Sheehy, G. R. R. Bell, L. M. Mäthger, S. L. Senft, T. J. Wardill, W. S. Lane, A. M. Kuzirian, R. T. Hanlon, E. L. Hu and K. K. Parker, *Journal of The Royal Society Interface*, 2014, **11**, 20130942.

7 T. L. Williams, S. L. Senft, J. Yeo, F. J. Martín-Martínez, A. M. Kuzirian, C. A. Martin, C. W. DiBona, C.-T. Chen, S. R. Dinneen, H. T. Nguyen, C. M. Gomes, J. J. C. Rosenthal, M. D. MacManes, F. Chu, M. J. Buehler, R. T. Hanlon and L. F. Deravi, *Nature Communications*, 2019, **10**, 1004.

8 L. M. Mäthger and R. T. Hanlon, *Cell and Tissue Research*, 2007, **329**, 179-186.

9 R. T. Hanlon, L. M. Mäthger, G. R. R. Bell, A. M. Kuzirian and S. L. Senft, *Bioinspiration & Biomimetics*, 2018, **13**, 035002.

10 L. Sumathirathne, T. Kim, D. Q. Bower and L. F. Deravi, *ECS Sensors Plus*, 2023, **2**, 023601.

11 S. A. Morin, R. F. Shepherd, S. W. Kwok, A. A. Stokes, A. Nemiroski and G. M. Whitesides, *Science*, 2012, **337**, 828-832.

12 P. A. Sullivan, D. J. Wilson, M. Vallon, D. Q. Bower and L. F. Deravi, *Advanced Materials Interfaces*, 2023, **10**, 2202463.

13 A. Kumar, T. L. Williams, C. A. Martin, A. M. Figueroa-Navedo and L. F. Deravi, *ACS Applied Materials & Interfaces*, 2018, **10**, 43177-43183.

14 M. Xiao, Y. Li, J. Zhao, Z. Wang, M. Gao, N. C. Gianneschi, A. Dhinojwala and M. D. Shawkey, *Chemistry of Materials*, 2016, **28**, 5516-5521.

15 Y. Zhang, J. Qiu, R. Hu, P. Li, L. Gao, L. Heng, B. Z. Tang and L. Jiang, *Physical Chemistry Chemical Physics*, 2015, **17**, 9651-9658.

16 X. Fei, T. Lu, J. Ma, W. Wang, S. Zhu and D. Zhang, *ACS Applied Materials & Interfaces*, 2016, **8**, 27091-27098.

17 I. Jurewicz, A. A. K. King, R. Shanker, M. J. Large, R. J. Smith, R. Maspero, S. P. Ogilvie, J. Scheerder, J. Han, C. Backes, J. M. Razal, M. Florescu, J. L. Keddie, J. N. Coleman and A. B. Dalton, *Advanced Functional Materials*, 2020, **30**, 2002473.

18 Y. Yue, T. Kurokawa, M. A. Haque, T. Nakajima, T. Nonoyama, X. Li, I. Kajiwara and J. P. Gong, *Nature Communications*, 2014, **5**, 4659.

19 S. J. Yeo, F. Tu, S.-h. Kim, G.-R. Yi, P. J. Yoo and D. Lee, *Soft Matter*, 2015, **11**, 1582-1588.

20 N. Vogel, S. Utech, G. T. England, T. Shirman, K. R. Phillips, N. Koay, I. B. Burgess, M. Kolle, D. A. Weitz and J. Aizenberg, *Proceedings of the National Academy of Sciences*, 2015, **112**, 10845-10850.

21 A. E. Goodling, S. Nagelberg, M. Kolle and L. D. Zarzar, *ACS Materials Letters*, 2020, **2**, 754-763.

22 Q. He, K. H. Ku, H. Vijayamohanan, B. J. Kim and T. M. Swager, *Journal of the American Chemical Society*, 2020, **142**, 10424-10430.

23 E. S. A. Goerlitzer, R. N. Klupp Taylor and N. Vogel, *Advanced Materials*, 2018, **30**, 1706654.

24 S. Park, H. Hwang, M. Kim, J. H. Moon and S.-H. Kim, *Nanoscale*, 2020, **12**, 18576-18594.

25 J.-G. Park, S.-H. Kim, S. Magkiriadou, T. M. Choi, Y.-S. Kim and V. N. Manoharan, *Angewandte Chemie International Edition*, 2014, **53**, 2899-2903.

26 S.-H. Kim, J.-G. Park, T. M. Choi, V. N. Manoharan and D. A. Weitz, *Nature Communications*, 2014, **5**, 3068.
27 T. M. Choi, J.-G. Park, Y.-S. Kim, V. N. Manoharan and S.-H. Kim, *Chemistry of Materials*, 2015, **27**, 1014-1020.
28 T. L. Williams, C. W. DiBona, S. R. Dinneen, S. F. Jones Labadie, F. Chu and L. F. Deravi, *Langmuir*, 2016, **32**, 3754-3759.
29 R. K. Shah, H. C. Shum, A. C. Rowat, D. Lee, J. J. Agresti, A. S. Utada, L.-Y. Chu, J.-W. Kim, A. Fernandez-Nieves, C. J. Martinez and D. A. Weitz, *Materials Today*, 2008, **11**, 18-27.
30 V. Hwang, A. B. Stephenson, S. Barkley, S. Brandt, M. Xiao, J. Aizenberg and V. N. Manoharan, *Proceedings of the National Academy of Sciences*, 2021, **118**, e2015551118.
31 S. R. Dinneen, R. M. Osgood, III, M. E. Greenslade and L. F. Deravi, *The Journal of Physical Chemistry Letters*, 2017, **8**, 313-317.
32 P. A. Rundquist, P. Photinos, S. Jagannathan and S. A. Asher, *The Journal of Chemical Physics*, 1989, **91**, 4932-4941.
33 J. S. Pedersen, *Advances in Colloid and Interface Science*, 1997, **70**, 171-210.
34 S. Magkiriadou, J.-G. Park, Y.-S. Kim and V. N. Manoharan, *Physical Review E*, 2014, **90**, 062302.
35 W. Tomal and J. Ortyl, *European Polymer Journal*, 2022, **180**, 111588.
36 A. Butenandt, U. Schiedt and E. Biekert, *Justus Liebigs Annalen der Chemie*, 1954, **588**, 106-116.
37 F. Figon, T. Munsch, C. Croix, M.-C. Viaud-Massuard, A. Lanoue and J. Casas, *Insect Biochemistry and Molecular Biology*, 2020, **124**, 103403.
38 M. Hori and L. M. Riddiford, *Insect Biochemistry*, 1981, **11**, 507-513.

This journal is © The Royal Society of Chemistry 20xx

Please do not adjust margins